32nd URSI GASS, Montreal, 19-26 August 2017

An X-band radio channel model for propagation through the solar corona

A.J. Stocker*(1), D.R. Siddle(1), E.M. Warrington(1), G. Mariotti(2)(5), D. Silvestri(2)(6), A. Zeqai(2), P. Tortora(2), A. Argyriou(3), J. De Vicente(4), R. Abello(4), and M. Mercolino(4)
(1) University of Leicester, U.K. (sto@le.ac.uk)
(2) University of Bologna, Italy
(3) University of Thessaly, Greece
(4) ESA, Darmstadt, Germany
(5) Now at SITAEL S.p.A.
(6) Now at Unisorting S.r.l.

Abstract

Spacecraft communication systems operating at X-band are strongly affected when the propagation path passes close to the sun. In this paper, a channel model that can generate a time-series of signal amplitude and phase is presented. The channel model reproduces the observations well for Sun-Earth-Probe (SEP) angles >2° and, with some caveats, works at smaller values of SEP.

1. Introduction

When the propagation path between the Earth and a distant spacecraft lies close to the sun, as it does during superior solar conjunctions (Figure 1), the coronal plasma can have severe effects on the communications channel through, for example, the introduction of amplitude and phase scintillations. While much work in this area concentrates on using the effects on signals to diagnose the condition of the solar plasma (e.g, [1, 2, 3]) other studies have developed to study the effect on communication systems (e.g. [4, 5, 6]) usually based on modelling the effects using a Rician distribution.

In this paper, a channel model based on experimentally derived power spectral densities for the phase and amplitude of X-band signals propagating through the solar corona during conjunction is described. For X-band, the results from the model are in close agreement with experimental observations at SEP>2° and, for some purposes, may be suitable down to SEP~1°.

2. Experimental observations

In order to derive the model, open-loop measurements of X-band signals radiated from the *Mars Express* spacecraft recorded during the Mars solar conjunction of 2013 while SEP<10° (4 March–26 May) were used. Example measurements of signal power and phase (corrected for dynamics) when SEP~2.4° are presented in Figure 2. The solar plasma causes the relatively low frequency amplitude scintillation and variations in phase while the faster variations are due to the thermal noise.

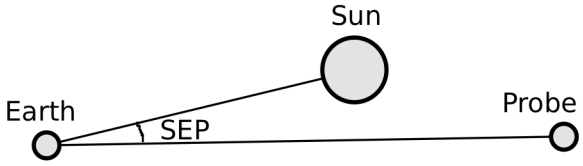

Figure 1. Geometry of Earth and spacecraft during superior solar conjunction.

In order to generate the amplitude PSD, the DC offset and any long-term trend in the amplitude time-series is removed by subtracting a straight line fit to the data, an FFT is applied to the resultant amplitude variations and the resultant spectrum converted to a PSD spectrum. An example PSD spectrum of the amplitude scintillation is presented in Figure 3 (the sharp cut off at 200 Hz results from the low-pass filter applied to the observations). Three parts to the spectrum have been identified:

1. A white noise component that corresponds to thermal noise is observed at frequencies higher than about 10 Hz. The PSD level associated with this region is independent of SEP provided the sun is not in an antenna lobe.
2. A second 'white noise' region where the PSD is flat as a function of frequency that corresponds to the scintillation introduced by the solar corona. This lies between $3x10^{-4}$ and 0.3 Hz, with a transition region

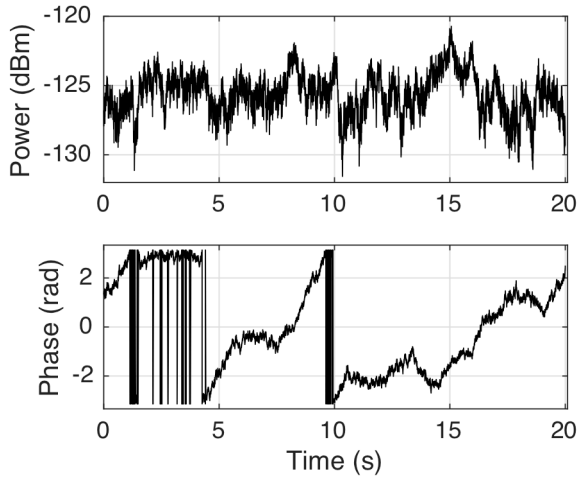

Figure 2. Plot of (top panel) signal power at the input to receiver and (bottom panel) phase observed on 7 April 2013 (SEP~2.4°). A low-pass filter has been applied to the open loop data with a cut off of 200 Hz.

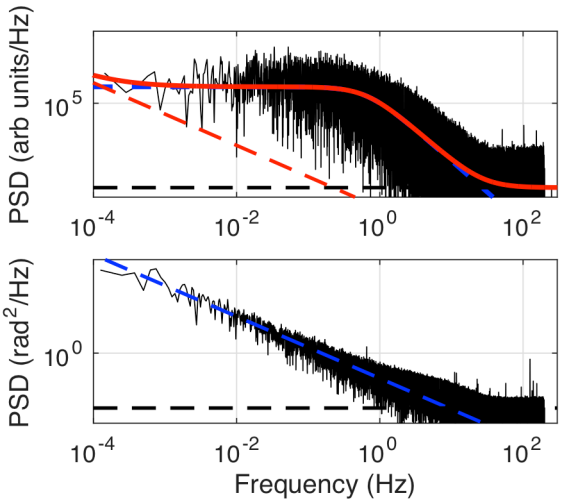

Figure 3. Power spectral density for (top panel) power and (bottom panel) phase on 7 April 2013 (SEP~2.4°). In the top panel, P_{GM} (blue dashed), P_{PN} (red dashed), P_{WN} (black dashed) and P (red solid) are presented. In the bottom panel, Pϕ (blue dashed) and $P\phi_{WN}$ (black dashed) are shown.

between this and the white noise at higher frequencies (i.e. between 1 and 10 Hz). The level and upper frequency are strongly dependent on SEP.

3. A pink noise (PN) component at lower frequencies (this is more evident for higher values of SEP than in this example). The PSD level of the PN does not appear to systematically depend on SEP, although there is some variation from pass to pass.

In order to model and synthesise the amplitude PSD, three functions have been combined and the least squares found in an iterative fit. The pink noise has been modelled such that the PSD level, P_{PN} is given by

$$\log_{10} P_{PN} = -f + c \qquad (1).$$

where f is the amplitude fluctuation frequency and c is a constant.

The PSD level of the solar channel has been modelled as a function of fluctuation frequency using a Gauss-Markov (GM) function such that

$$\log_{10}(P_{GM}) = \log_{10}\left(\frac{L_{GM}{}^2 f_{GM}}{(2\pi f)^2 + f_{GM}{}^2}\right) \qquad (2).$$

where L_{GM} is the Gauss-Markov level and f_{GM} is the coherence frequency.

The PSD level of the white noise, P_{WN} is independent of fluctuation frequency.

In the course of fitting, since the pink noise does not vary systematically with SEP the value of c (i.e. P_{PN} at 1 Hz) has been taken as a fixed parameter while the others are free parameters. The overall PSD is given by:

$$P = P_{PN}(f) + P_{GM}(f) + P_{WN} \qquad (3).$$

The frequency spectrum of the phase fluctuations is calculated in a number of stages broadly following the method of [1]:

1. The unwrapped phase values of the frequency corrected signal are pre-whitened using the difference between successive samples and multiplying this by the sample rate to convert from radians per sample to radians per second
2. A Hamming window, then an FFT, is applied
3. The spectrum is then corrected by the gain associated with the Hamming window and for single sided symmetry, and then re-reddened. The sharp cut off at 200 Hz is because of the low-pass filter.

The phase scintillation PSD intensity, Pϕ is given by

$$\log_{10} P_{\phi} = m \log_{10} f + c \qquad (4).$$

where, f is the fluctuation frequency and m and c are the gradient and intercept, respectively. A thermal white noise component is also present ($P\phi_{WN}$).

3. Model

3.1 Amplitude scintillation

The parameters for the thermal white noise (WN), pink noise (PN), and solar coronal effects from Equations 1–3 found at a range of SEP values (between 0.9° and 10°) are plotted in Figure 4. The PN was the fixed parameter and was fairly constant from pass-to-pass, and has been assumed to be independent of SEP. However, the pass-to-pass variation has been accounted for by taking the upper and lower deciles of the observations to represent 'poor' (high values) and 'good' (low values) conditions. The value of L_{GM} increases fairly linearly as SEP is decreased (note that this is a log-log plot) except for the two lowest values of SEP. Three regions have been identified and a best fit applied to each as follows:

For SEP≤1.556°

$$\log_{10}(L_{GM}) = -0.746 \log_{10}(SEP) + 7.4000 \qquad (5a).$$

For 1.556<SEP≤10°

$$\log_{10}(L_{GM}) = 4.044 (\log_{10}(SEP))^2 - 8.985 \log_{10}(SEP) + 8.832 \qquad (5b).$$

For SEP>10°

$$\log_{10}(L_{GM}) = -0.879 \log_{10}(SEP) + 4.770 \qquad (5c).$$

Some variation in the L_{GM} values is observed and this has been accounted for in the model by calculating the upper and lower deciles of the difference between the experimental values and the model values and assigning these to 'poor' and 'good' versions of the channel.

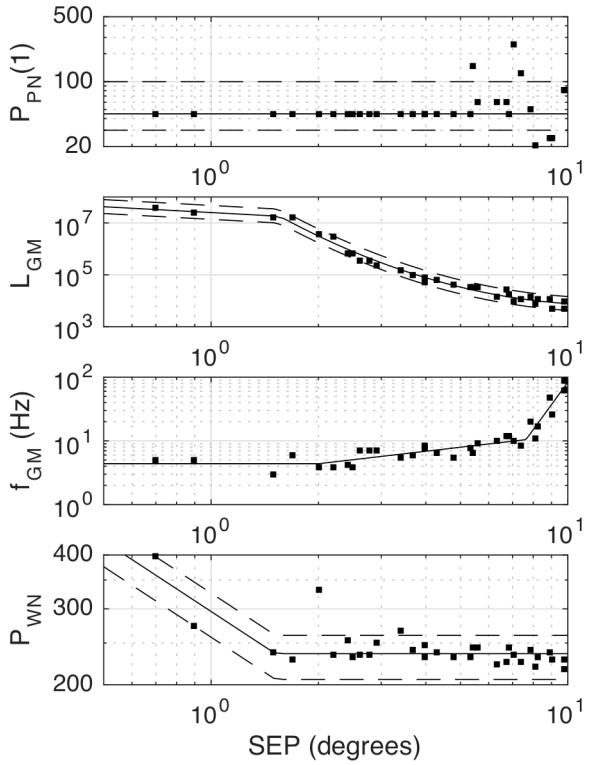

Figure 4. The experimentally derived amplitude scintillation best-fit parameters as a function of SEP for (from the top) pink noise level at 1 Hz, Gauss-Markov level, Gauss-Markov coherence frequency, and white noise level. The best-fit (solid line) and deciles (dashed lines) are also shown.

There is a decrease in f_{GM} with decreasing SEP (again, note the log-log axes). A model with three SEP ranges has been developed.

For SEP<2.0°

$$f_{GM} = 4.38 \qquad (6a).$$

For 2≤SEP<7.633°

$$\log_{10}(f_{GM}) = 0.651\log_{10}(SEP) + 0.445 \qquad (6b).$$

While for SEP≥7.33°

$$\log_{10}(f_{GM}) = 7.678\log_{10}(SEP) - 5.758 \qquad (6c).$$

We have assumed that the trend in f_{GM} continues for SEP>10°, although we have no observations to test this against (the model predicts that the solar plasma effects rapidly become weaker at higher values of SEP). Although it is likely that increasing f_{GM} for a fixed value of L_{GM} would increase the level of scintillation, we have not provided a range of values for this parameter (i.e. no 'poor' or 'good' values) since the two values are coupled in how much scintillation arises.

Finally, the value of P_{WN} is fairly constant except at small values of SEP. For SEP<1.51°

$$\log_{10}(P_{WN}) = -0.5430\log_{10}(SEP) + 2.471 \qquad (7a).$$

For SEP≥1.51

$$P_{WN} = 236.1 \qquad (7b).$$

Upper and lower decile values of $1.1030P_{WN}$ and $0.8716P_{WN}$ provide the values for 'poor' and 'good' channels, respectively.

3.2 Phase scintillation

The values of m and c (see Equation 4) have been fitted to the observations for each pass and the results plotted as a function of SEP in Figure 5. The variation of both m and c with SEP are linear with best-fit equations given as follows

SEP>10°

$$m = -2.612 \qquad (8a).$$

SEP≤10°

$$m = 0.0112 \times SEP - 2.724 \qquad (8b).$$

For SEP<4.7°

$$c = -4.4370 \times SEP - 0.4336 \qquad (9a).$$

while for SEP≥4.7°

$$c = -1.9516 \times SEP - 2.1085 \qquad (9b).$$

In order to reflect the pass-to-pass variation of c, the upper and lower deciles of variations from the 'moderate' value given in the above equations have been adopted.

The thermal white noise component of the phase PSD, $P\phi_{WN}$ is characterized as the mean level (Figure 3). $P\phi_{WN}$ has been calculated for each pass and plotted as a function of SEP in Figure 5. There is a weak dependence on SEP and the best fit for SEP<10° is given by

$$\log_{10}(P\phi_{WN}) = -0.0049 \times SEP - 4.7729 \qquad (10).$$

For SEP>10°, we have assumed that the log of the white noise intensity is constant with a value of –4.82. The upper and lower deciles of the difference of the measurements from the equation given above have been used to characterise the good and poor channel behaviour.

3.3 Creating a synthetic time series

In order to synthesize an artificial amplitude or phase time-series, the following steps are taken

1. The PSD parameters are generated for a given SEP and channel quality using the models described above
2. The PSD is created with the desired sample rate and duration (i.e. the inverse of the lowest frequency).
3. This produces a curve like the overall line in Figure 3. In order to produce a different time series each time the model is run, the phase of each sample in the PSD spectrum is randomised.
4. The inverse FFT of the resultant PSD is then found to produce the time series.

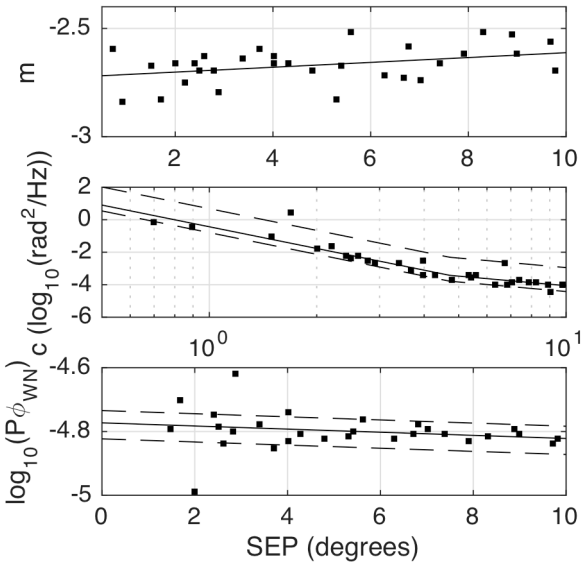

Figure 5. (top to bottom) The variation of m, c, and $P\phi_{WN}$ as a function of SEP. The solid lines correspond to the 'moderate' channel behaviour and the dashed lines to 'poor' (upper line) and 'good' (lower line).

Some examples of the outcome of this process for the same conditions as for the observations presented in Figure 2 are presented in Figure 6. These time series are highly reminiscent of the ones observed and they have similar properties, e.g. the experimental value of the amplitude scintillation index is 0.34, while the simulated value is 0.36.

4. Concluding remarks

A channel model for X-band signals propagating through the solar corona has been derived from the behaviour of experimentally determined power spectral densities of the variation in signal amplitude and phase. The time series of amplitude and phase obtained from the model have similar characteristics (e.g. amplitude scintillation index, signal distributions, etc.) to the observed values. The results can be scaled to other frequencies (e.g. S-band and Ka-band) and to other systems (e.g. by changing the SNR). However, there are limits to the applicability of the model. For example, the model currently does not include the phase slips associated with deep fades during strong scintillation. However, in 2013 for X-band, this was not a problem provided SEP>2.1° since this is the highest value of SEP for which phase slips are present. For lower values of SEP, the model will currently produce over-optimistic performance data since, for example, the phase slips will cause significant errors in the tracking capability of a PLL. Another problem with the model for conditions of strong scintillation is Gaussian distributions produced by the PSD method since these should be skewed for these conditions.

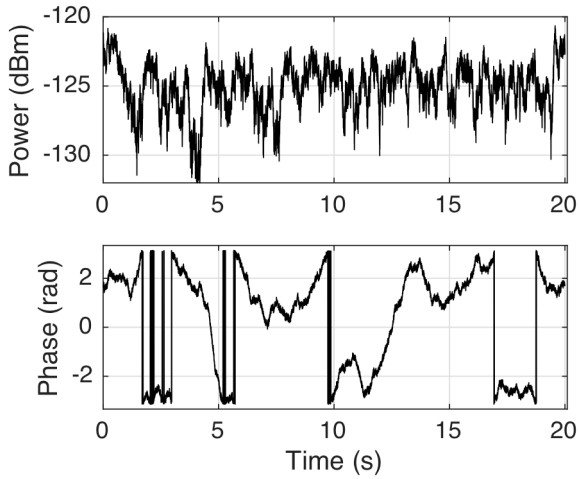

Figure 6. Synthetic time series of (top panel) signal power and (bottom panel) phase for a 'poor' channel at SEP=2.4°. The sample rate is 400 samples per second.

5. Acknowledgements

This work (HELIOS – Highly rEliable LInks during sOlar conjunctionS) has been funded by the General Study Programme (GSP) of the European Space Agency under Invitation To Tender Reference: AO/1-8050/14/F/MOS

6. References

1. R. Woo, F.C. Yang, and K.W. Yip, "Measurements of large-scale density fluctuations in the solar wind using dual-frequency phase scintillations", *The Astrophysical Journal*, 210:568–574, 1976.

2. M. Pätzold, *et al.*, "Coronal density structures and CMEs: Superior solar conjunctions of Mar Express, Venus Express, and Rosetta: 2004, 2006, and 2008", *Solar Phys* 279:127-152, DOI 10.1007/s11207-012-9991-y, 2012.

3. A.K. Verma, *et al.*, "Electron density distribution and solar plasma correction of radio signals using MGS, MEX, and VEX spacecraft navigation data and its application to planetary ephemerides", *Astronomy and Astrophysics* 550, DOI: 10.1051/0004-6361/201219883, 2012.

4. D.D. Morabito, *et al.*, "The Cassini 2000 solar conjunction", *IEEE Trans. on Antennas and Propagation*, 51, 201–219, DOI 10.1109/TAP.2003.809055, 2003.

5. D.D. Morabito, "Solar-induced fluctuations on spacecraft signal amplitude observed during solar superior conjunctions of the Cassini spacecraft", *Radio Sci*, 42, RS3002, doi:10.1029/2005RS003425, 2007.

6. Q. Li *et al.*, "Performance study of a deep space communications system with low-density parity-check coding under solar scintillation", *International Journal of Communications*, 6, 2012.